RAPID COMMUNICATIONS

PHYSICAL REVIEW E VOLUME 48, NUMBER 5 NOVEMBER 1993

Thermal convection in a planar nematic liquid crystal with a stabilizing magnetic field

Lars Inge Berge, Guenter Ahlers, and David S. Cannell

Department of Physics and Center for Nonlinear Science, University of California, Santa Barbara, California 93106

(Received 27 April 1993; revised manuscript received 11 June 1993)

We report experimental results for thermal convection in a horizontal layer of a planar nematic liquid crystal [4-*n*-pentyl-4'-cyanobiphenyl (5CB)] heated from below in a uniform horizontal magnetic field **H**. The threshold for convection and the critical wave-vector components were measured as a function of H. The convection rolls were oriented with their axes normal (oblique) to the field direction for $H < H_{L1}$ ($H_{L1} < H < H_{L2}$), where H_{L1} and H_{L2} are the lower and upper Lifshitz fields, respectively. Above H_{L2} the orientation was parallel to **H**. The dependence of the orientation on H near H_{L1} and H_{L2} agrees with theoretical predictions.

PACS number(s): 47.20.Bp, 47.27.Te

During the last two decades a great deal has been learned from experiments about nonlinear pattern-forming dissipative systems [1]. Of particular interest at the present are patterns that form in two spatial dimensions. Most of these have been studied in systems that are isotropic in the plane of the pattern. Notable examples are Rayleigh-Bénard convection (RBC) in an isotropic fluid and the formation of Turing patterns in chemical reactions [1]. In those cases the pattern, e.g., the convection rolls or hexagons in RBC, can form with an arbitrary angular orientation which should be irreproducible in successive independent experiments unless the boundary conditions imposed by the apparatus break the rotational symmetry. However, it is of interest also to examine systems that have an *intrinsic* anisotropy which singles out a particular angular orientation $\hat{\mathbf{n}}$. This anisotropy introduces new bifurcation phenomena, which are absent in the isotropic case because the orientation of the pattern relative to $\hat{\mathbf{n}}$ can now change as a control parameter is varied. Examples of anisotropic systems are nematic liquid crystals in which the director (the average direction of alignment of the elongated molecules) is oriented in a particular direction parallel to flat plates which confine the fluid [2]. We will discuss pattern formation in a thin horizontal layer of a nematic liquid crystal heated from below and exposed to a horizontal magnetic field **H** parallel to $\hat{\mathbf{n}}$ [3–10]. This system was studied theoretically by Feng, Pesch, and Kramer [11]. Over an appropriate parameter range, RBC rolls are expected to form with an amplitude that grows continuously from zero as the temperature difference ΔT is increased beyond its threshold value ΔT_c. The orientation of the roll axis is predicted to depend upon H. As H is increased beyond a critical value H_{L1}, the roll-axis orientation at onset changes continuously from being normal to $\hat{\mathbf{n}}$ and **H** (normal rolls) to being oblique to $\hat{\mathbf{n}}$ and **H** (oblique rolls). When H reaches values beyond a second critical value H_{L2}, the orientation is parallel to **H** and $\hat{\mathbf{n}}$. In analogy to equilibrium critical phenomena [12], the two-parameter bifurcation points at which the transitions from normal to oblique and oblique to parallel rolls occur have been called Lifshitz points [13]. We present quantitative measurements of the roll orientation as H is increased from below H_{L1} to above H_{L2}. We also report results for $\Delta T_c(H)$ over a wide range of H. Our results are in quantitative agreement with the calculations by Feng, Pesch, and Kramer [11], whose theoretical work motivated our experiments.

We used the liquid crystal 5CB (4-*n*-pentyl-4'-cyanobiphenyl). It had a nematic phase below $T_{NI} = 35.0\,^{\circ}\mathrm{C}$ (T_{NI} is the nematic-isotropic transition temperature), with a positive anisotropy of the diamagnetic susceptibility χ_a which assures that a monodomain sample will form with $\hat{\mathbf{n}}$ parallel to **H** when H is sufficiently large. Near the top and bottom this alignment was reinforced by surface treatment of the confining plates. 5CB also has an anisotropic thermal conductivity, with $\lambda_{\parallel} > \lambda_{\perp}$ ($\lambda_{\parallel}$ and $\lambda_{\perp}$ are the conductivities parallel and perpendicular to $\hat{\mathbf{n}}$, respectively). This leads to focusing of the heat current when a director fluctuation occurs. Some of the ensuing horizontal temperature fluctuations are destabilizing, and thus lower the convective threshold relative to that of an isotropic fluid [4]. At large H, the destabilizing fluctuations are suppressed, and the system has the same onset as an isotropic fluid.

We built an apparatus to measure the convective heat transport with high precision and to visualize the pattern for $H \lesssim 1500$ G. We used three experimental cells. One (cell 1) was rectangular with a width $L_1 = 3.86$ cm, length $L_2 = 7.72$ cm, and height $d_1 = 0.498$ cm. The other two (cells 2 and 3) were cylindrical with equal radii $r = 4.19$ cm and heights $d_2 = 0.404$ and $d_3 = 0.327 \pm 0.0015$ cm, respectively. The majority of the measurements were made in cell 2. For cell 1, both **H** and $\hat{\mathbf{n}}$ were parallel to the long side. The sidewalls were made of Delrin. The top was a 0.33-cm-thick sapphire, and the bottom was a 1.11-cm-thick aluminum plate. Before filling the cells, the heights were examined interferometrically and found to vary less than 2 μm. The top-plate temperature for cells 1 and 2 (cell 3) was kept constant within 0.001 °C near 25.80 °C (20.00 °C) by temperature-controlled flowing water [14]. Constant power was applied to the bottom plate. The apparatus was placed between the pole pieces of an electromagnet with a 23.5-cm-wide pole gap. Uniform fields ($\pm 0.15\%$) were achieved by using pole pieces with concave surfaces. Apparatus parts were machined from aluminum and then HCR magnaplated (General Magnaplate Corp.) to achieve a nonmagnetic system with adequate corrosion resistance. A computer-interfaced video camera was used to view the convection patterns. The samples were nontransparent, but any flow

that distorted the director field near the sample top became visible because the director distortion affected the diffuse scattering of ambient light by the nematic liquid crystal. The heat-transport measurements will be expressed as the Nusselt number, equal to the effective conductivity of the fluid layer divided by $\lambda_\perp$.

For 5CB, most material parameters have been measured [15–24], and we list them in a footnote [25]. There are two control parameters for our system. One is the Rayleigh number $R=\alpha g d^3 \Delta T/(\alpha_4/2\rho)\kappa_\perp$, where g is the gravitational acceleration, α is the isobaric thermal expansion coefficient, $\alpha_4/2\rho$ corresponds to the isotropic kinematic viscosity, and $\kappa_\perp$ is the perpendicular thermal diffusivity. The other is the magnetic-field strength H scaled by the Fréedericksz field $H_F=(\pi/d)(k_{11}/\chi_a\rho)^{1/2}$, i.e., $h=H/H_F$. Here k_{11} is the splay elastic constant and χ_a is the anisotropy of the diamagnetic susceptibility. At 27 °C, we expect [25] $H_F=14.2$, 17.5, and 21.6±0.4 G for cells 1, 2, and 3, respectively.

The onset of convection and the nature of the bifurcation were determined from the Nusselt numbers N. Figure 1 shows N at several fields for cell 2. Data taken with increasing and decreasing heat current show no hysteresis within our resolution at the *primary* bifurcation, although hysteretic secondary bifurcations are suggested by most of the data. Measurements at $H\simeq 1000$ G for cells 1, 2, and 3 give $\Delta T_c=2.87$, 5.25, and 11.82 K, corresponding to [25,26] $R_c=1640$, 1720, and 1740, respectively. In this high-field region, the director is still expected to determine the roll orientation, but the threshold R_c should be the same ($R_c=1708$) as that of an isotropic fluid. Clearly, there is excellent agreement between experiment and theory.

In the high-field limit, the slope $S\equiv(N-1)/\epsilon$ with $\epsilon\equiv\Delta T/\Delta T_c-1$ is 1.0, 1.29, and 1.58 for cells 1, 2, and 3, respectively. The results for cells 1 and 2 differ significantly from the calculated value [11] 1.5. The difference is likely to be due to the finite size of the containers. Measurements of S with pure fluids in circular cells of aspect ratios similar to that of cell 2, for instance, [14] have also given values of S somewhat below the theoretical prediction [27] for the laterally infinite system. The slope for cell 3 may well be influenced by non-Boussinesq effects because the temperature differences are quite large. For cell 2, S was studied in some detail as a function of H. As H decreased, S increased and seemed to diverge near $H\simeq 500$ G. However, we have been unable to find any hysteresis in N for smaller H, as might have been expected if the bifurcation had become subcritical. Instead, the data suggest that the initial slope of N remains large over a range of H. For $H\lesssim 350$ G, S becomes finite once more, but it now has a value near 0.6.

The dependence upon h of the measured ΔT_c is compared with theory in Fig. 2. We show as squares, circles, and crosses, respectively, the ratio $R_c(h)/R_c(\infty)$ for cells 1, 2, and 3. Their good agreement with each other is consistent with the expected scaling of H with H_F. The solid line is the theoretical prediction [11]. Since the calculation contains no adjustable parameters, the agreement between theory and experiment is impressive.

Figure 3 shows images of the patterns at small ϵ for various H and for cell 1. At small H [3(a) and 3(b)], the rolls are normal to the director and the field, and the wave number $|k|$ decreases with increasing H. It should be noted that $|k|$ tends to change discontinuously, since structures commensurate with the cell width seem to be preferred. As H is further increased, we pass the predicted [11] Lifshitz point where there is a continuous transition to oblique rolls. The oblique rolls could have either of two orientations, corresponding to a positive or negative angle between their axis and $\hat{\mathbf{n}}$. Over an appropriate parameter range with angles close to $\pi/4$, the coexistence of both orientations as a bimodal structure was observed [Fig. 3(d)]. At the slightly higher field of 442 G [Fig. 3(e)] no bimodal structure was found for $\epsilon<0.07$. Compared to patterns in pure fluids, the rolls seem surprisingly little

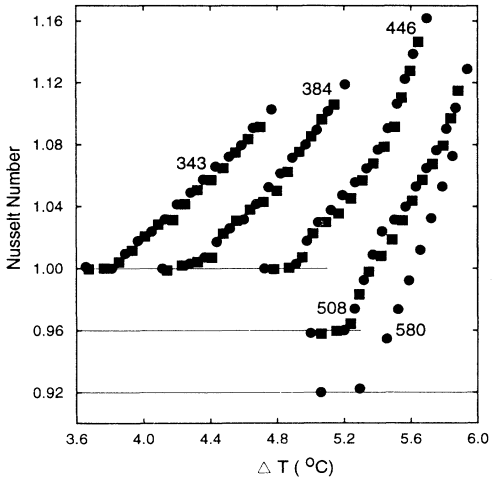

FIG. 1. Nusselt number measurements for cell 2 at the field values (in gauss) indicated in the figure (the dimensionless fields are obtained by dividing by $H_F=17.5$ G). The circles (squares) correspond to data taken after increasing (decreasing) the heat current. The results at 580 and 508 G were displaced downward by 0.08 and 0.04, respectively.

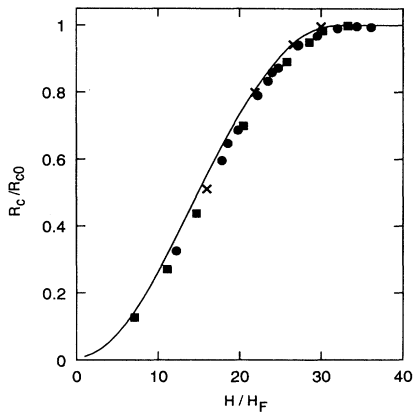

FIG. 2. Experimental and theoretical [11] results for the reduced critical Rayleigh number $R_c(H)/R_{c0}$ as a function of the reduced field H/H_F. The vertical scale is set by $R_{c0}=R_c(H=\infty)\simeq 1708$. The horizontal scale is determined by the Fréedericksz field H_F. The squares, circles, and crosses are for cells 1, 2, and 3, respectively. The solid line is the theoretical prediction.

affected by the sidewalls, although there is a tendency for them to terminate with their axes perpendicular to **H**, as can be seen in Figs. 3(c) and 3(e).

Figure 4 shows patterns for cell 2 and $\epsilon \simeq 0.01$. Images for cell 3 look similar. Again we see the transition as a function of H from normal to oblique rolls. Near the lower Lifshitz field H_{L1}, both roll orientations coexist in our cell, each occupying a different portion with a boundary between them across the diameter parallel to **H**, as seen for 425 and 441 G. For the field range where oblique rolls at an angle close to $\pi/4$ to **H** are expected, we once more observe bimodal structures near onset, as seen for 477 G. At higher fields only one mode exists, but either orientation occurs as shown by the images for 518 and 549 G. Above H_{L2}, no patterns were visible because the flow did not distort the director field. However, in this parameter range the flow became visible when the temperature at the cell bottom exceeded T_{NI} by a small amount; such experiments confirmed that the convection at high fields did indeed consist of parallel rolls [see Fig. 3(a) of Ref. [28]].

We determined the two components q_c and p_c of the

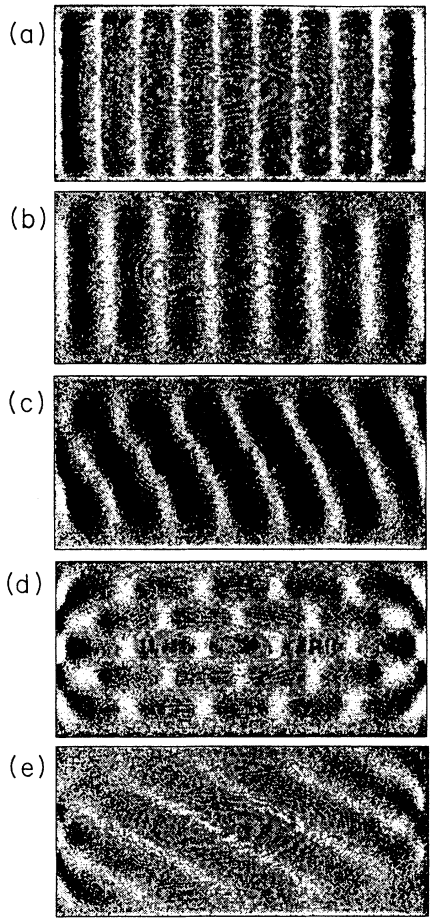

FIG. 3. Images of convection patterns in cell 1 for (a) 211 G at $\epsilon=0.036$, (b) 327 G at $\epsilon=0.005$, (c) 379 G at $\epsilon=0.035$, (d) 427 G at $\epsilon=0.069$, and (e) 442 G at $\epsilon=0.040$ (the dimensionless fields are obtained by dividing by $H_F=14.2G$). The oval fringes which may be visible in some of the images originate from the optics and do not correspond to any feature in the fluid flow.

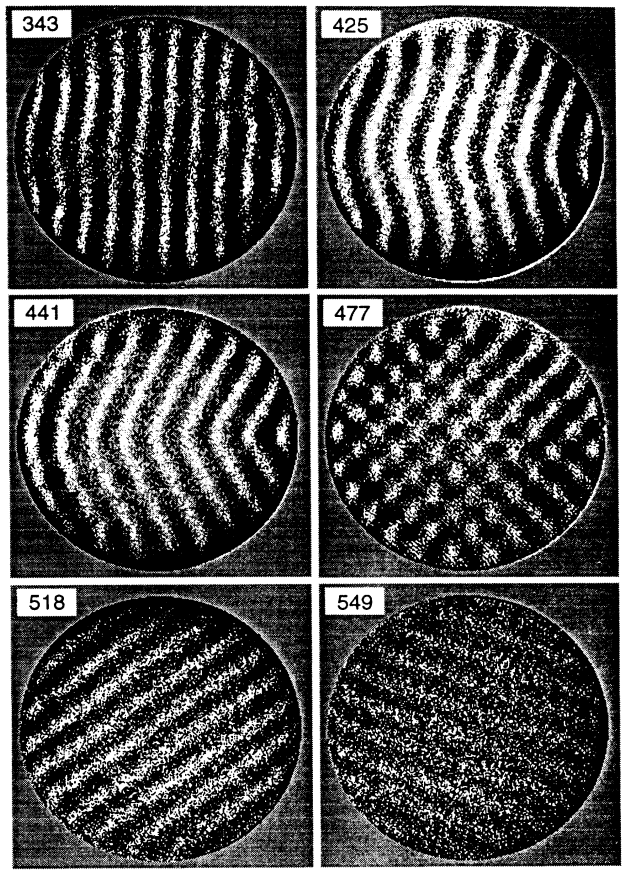

FIG. 4. Images of convection patterns for cell 2 at $\epsilon \simeq 0.01$. The numbers in the figure give the field values in gauss.

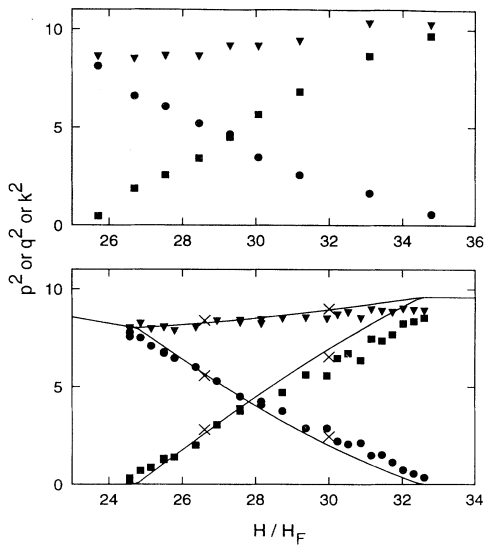

FIG. 5. The square of the modulus k and of the components q (parallel to $\hat{\mathbf{n}}$) and p (perpendicular to $\hat{\mathbf{n}}$) of the critical wave vector as a function of H/H_F. The upper figure is for cell 1. The lower one is for cells 2 and 3, and for the theory (solid lines). For cells 1 and 2, k^2, q^2, and p^2 are given as triangles, circles, and squares, respectively. The results for cell 3 are given as crosses.

critical wave vector $\mathbf{k}_c$ in the direction $\hat{\mathbf{n}}$ and perpendicular to $\hat{\mathbf{n}}$, respectively, as a function of H [29]. Figure 5 shows q_c^2, p_c^2, and k_c^2 and the corresponding theoretical [11] curves. The lower Lifshitz point is located at the field value at which p_c^2 begins to grow from zero, and the upper Lifshitz point corresponds to the field where q_c^2 vanishes. The Lifshitz points for cell 1 are 5–10% higher than those for cells 2 and 3, suggesting that the orientation of the boundaries relative to the pattern has an influence on the roll orientation. There is quantitative agreement between the measurements for cells 2 and 3 and theory [11]. From Fig. 5 it is apparent that p_c^2 (q_c^2) varies linearly with H near H_{L1} (H_{L2}). The implied square-root dependence of p_c and q_c on H near H_{Li} is in agreement with general theoretical predictions [12] for Lifshitz points.

In conclusion, our experiments have reproduced the predicted [12] square-root dependence of the wave-vector components upon the field near Lifshitz points. Detailed calculations by Feng, Pesch, and Kramer [11] are also confirmed very well.

We thank Q. Feng, W. Pesch, and L. Kramer for calling our attention to this interesting system, and for providing us with the program for the calculation of the theoretical results shown in Figs. 2 and 5. We gratefully acknowledge G. Ramian for designing the magnet pole pieces. We thank E. Bodenshatz and M. Dominguez-Lerma for useful discussions, and S. Morris and B. Frisken for their contributions to our understanding of nematic liquid crystals. This research was supported by the Department of Energy through Grant No. DOE FG03-87ER13738. One of us (L.I.B.) gratefully acknowledges the financial support of the Norwegian Research Council for Science and the Humanities.

[1] For a recent review, see for instance, M. C. Cross and P. C. Hohenberg, Rev. Mod. Phys. **65**, 851 (1993).

[2] P. G. de Gennes, *The Physics of Liquid Crystals* (Clarendon, Oxford, 1973).

[3] A small number of previous experiments [4–8] on RBC in nematics were reviewed recently by Barrat [9]. They mostly addressed issues other than those of interest here, such as the possibility of convection when heating from above, and the existence of subcritical and Hopf bifurcations in some parameter ranges.

[4] E. Dubois-Violette, E. Guyon, and P. Pieranski, Mol. Cryst. Liq. Cryst. **26**, 193 (1973).

[5] P. Pieranski, E. Dubois-Violette, and E. Guyon, Phys. Rev. Lett. **30**, 736 (1973).

[6] E. Guyon, P. Pieranski, and J. Salan, J. Fluid. Mech. **93**, 65 (1979).

[7] J. Salan and E. Guyon, J. Fluid. Mech. **126**, 13 (1983).

[8] K. Otnes and T. Riste, Physica **120B**, 376 (1983).

[9] R. J. Barratt, Liquid Crystals **4**, 223 (1989).

[10] Much has been done on electroconvection in a thin layer of a nematic liquid crystal in the presence of an electric field [see, for example, the review by I Rehberg, B. L. Winkler, M. de la Torre-Juarez, S. Rasenat, and W. Schöpf, Festkörperprobleme **29**, 35 (1989)]. As discussed, for instance, by Rehberg *et al.*, and by R. Ribotta, A. Joets, and L. Lei, Phys. Rev. Lett. **56** 1595 (1986), that system also produces a transition from normal to oblique rolls, but the roll orientation as a function of the relevant control parameter does not vary as expected [12] for a Lifshitz point. Reasons for this may be found in the fact that the transition, at least for some parameter ranges, is first order (subcritical) rather than continuous [see I. Rehberg, S. Rasenat, M. de la Torre-Juarez, W. Schöpf, F. Hörner, G. Ahlers, and H. R. Brand, Phys. Rev. Lett. **67**, 596 (1991)], and that it is a Hopf bifurcation (see Rehberg *et al.*).

[11] Q. Feng, W. Pesch, and L. Kramer, Phys. Rev. A **45**, 7242 (1992).

[12] R. M. Hornreich, M. Luban, and S. Shtrikman, Phys. Rev. Lett. **35**, 1678 (1975).

[13] W. Zimmermann and L. Kramer, Phys. Rev. Lett. **55**, 402 (1985).

[14] C. W. Meyer, G. Ahlers, and D. S. Cannell, Phys. Rev. A **44**, 2514 (1991).

[15] D. A. Dunmur and W. H. Miller, J. Phys. (Paris) Colloq. **40**, C3-141 (1979).

[16] J. Thoen, in *Phase Transitions in Liquid Crystals*, edited by S. Martellucci (Plenum, New York, 1992).

[17] G. S. Iannacchione and D. Finotello, Phys. Rev. Lett. **69**, 2094 (1992).

[18] P. L. Sherrell and D. A. Crellin, J. Phys. (Paris) Colloq. **40**, C3-211 (1979).

[19] M. J. Bradshaw, E. P. Raynes, J. D. Bunning, and T. E. Faber, J. Phys. (Paris) **46**, 1513 (1985).

[20] H. J. Coles and M. S. Sefton, Molec. Cryst. Liq. Cryst. Lett. **1**, 151 (1985).

[21] H. Kneppe, F. Schneider, and N. K. Sharma, Ber Bunsenges. Phys. Chem. **85**, 784 (1981).

[22] K. Skarp, S. T. Lagerwall, and B. Stebler, Mol. Cryst. Liq. Cryst. **60**, 215 (1980).

[23] H. J. Coles and M. S. Sefton, Molec. Cryst. Liq. Cryst. Lett. **3**, 63 (1986).

[24] G. Ahlers, D. S. Cannell, L. I. Berge, and S. Sakurai, Phys. Rev. E (to be published).

[25] The values listed here are for 27 °C. We have $\rho=1.021$ g/cm^3 and $\alpha=9.24\times10^{-4}$ K^{-1} [15], $C_p=1.94$ J/g K [16,17], $\chi_a=1.11\times10^{-7}$ cm^3/g [18], $(k_{11},k_{22},k_{33})=5.71,3.62,7.44)\times10^{-7}$ dyn s [19,20], and $(\alpha_1,\ldots,\alpha_6)=(-0.056,-0.711,-0.040,0.607,0.575,-0.174)$ dyn s/cm^2 [21–23]. From our measurements we get [24] $\lambda_\perp=1.326\times10^4$ erg/s cm K. We measured $\lambda_\parallel$ by applying a vertical field, and found [24] $\lambda_\parallel/\lambda_\perp=1.663$. Reasonable estimates of the uncertainties are 10% for α, 2% for χ_a, $\lambda_\perp$, k_{11}, and k_{33}, 4% for k_{22}, the larger of 10% or 0.01 dyn s/cm^2 for the α_i's (but with the Onsager relation $\alpha_2+\alpha_3=\alpha_6-\alpha_5$ preserved), and 0.5% for $\lambda_\parallel/\lambda_\perp$.

[26] In the same apparatus with water as the fluid, using a cell with the same L_1 and L_2 as cell 1 but with $d=0.477$ cm, we obtained $R_c=1690\pm40$.

[27] A. Schlüter, D. Lortz, and F. Busse, J. Fluid Mech. **23**, 129 (1965).

[28] G. Ahlers, L. I. Berge, and D. S. Cannell, Phys. Rev. Lett. **70**, 2399 (1993).

[29] For cell 1, we simply measured the angle in the images. For cells 2 and 3, we located the maxima in the modulus of the Fourier transform.

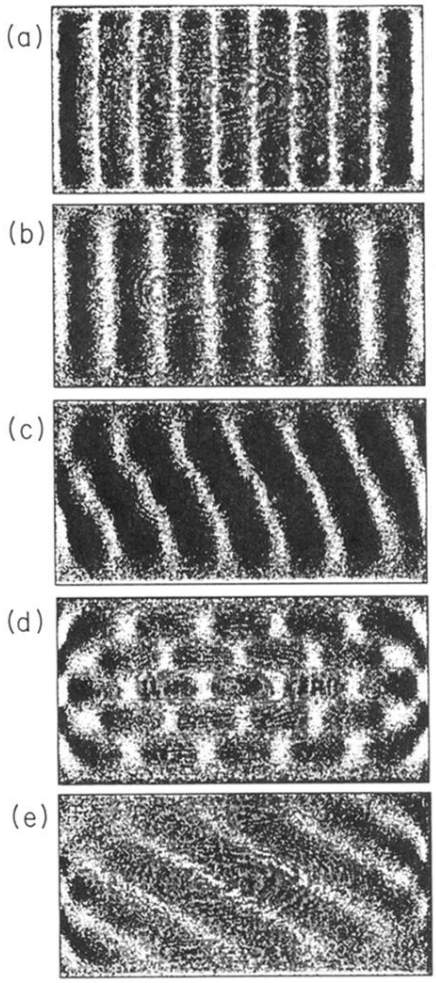

FIG. 3. Images of convection patterns in cell 1 for (a) 211 G at $\epsilon=0.036$, (b) 327 G at $\epsilon=0.005$, (c) 379 G at $\epsilon=0.035$, (d) 427 G at $\epsilon=0.069$, and (e) 442 G at $\epsilon=0.040$ (the dimensionless fields are obtained by dividing by $H_F=14.2G$). The oval fringes which may be visible in some of the images originate from the optics and do not correspond to any feature in the fluid flow.

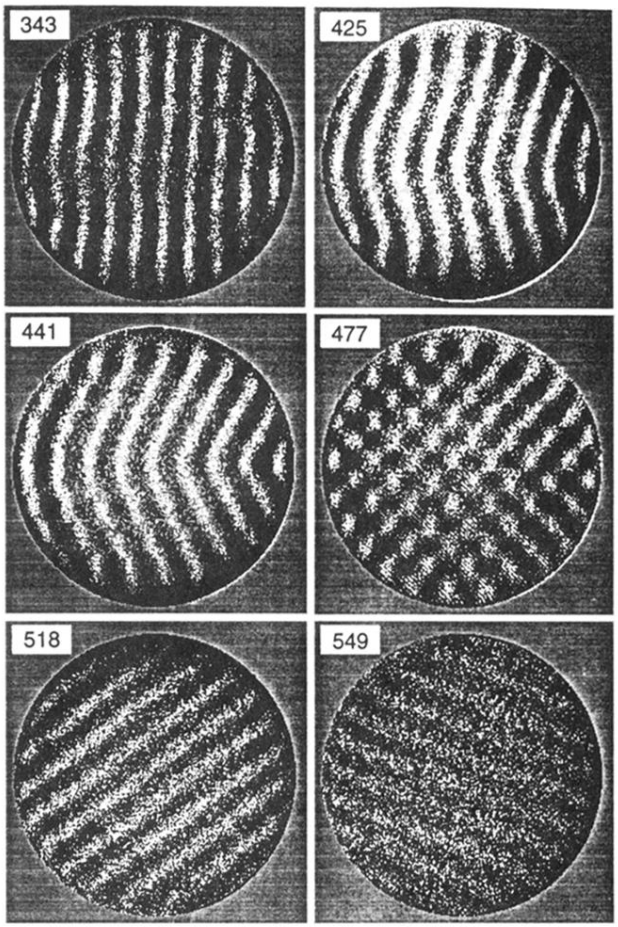

FIG. 4. Images of convection patterns for cell 2 at $\epsilon \simeq 0.01$. The numbers in the figure give the field values in gauss.